ADVANCED FUNCTIONAL MATERIALS
www.afm-journal.de

Programmable Macroporous Photonic Crystals Enabled by Swelling-Induced All-Room-Temperature Shape Memory Effects

*Sin-Yen Leo, Yongliang Ni, Can Xu, Yifan Zhang, Yuqiong Dai, Pengxu Qi, Angela T. Xie, Vito Basile, Curtis Taylor, and Peng Jiang**

This study reports unconventional, all-room-temperature shape memory (SM) effects using templated macroporous shape memory polymer (SMP) photonic crystals comprising a glassy copolymer with high-glass transition temperature. "Cold" programming of permanent periodic structures into temporary disordered configurations can be achieved by slowly evaporating various swelling solvents (e.g., ethanol) imbibed in the interconnecting macropores. The deformed macropores can be instantaneously recovered to the permanent geometry by exposing it to vapors and liquids of swelling solvents. By contrast, nonswelling solvents (e.g., hexane) cannot trigger "cold" programming and SM recovery. Extensive experimental and theoretical investigations reveal that the dynamics of swelling-induced plasticizing effects caused by fast diffusion of solvent molecules into the walls of macropores with nanoscopic thickness dominate both "cold" programming and recovery processes. Importantly, the striking color changes associated with the reversible SM transitions enable novel chromogenic sensors for selectively detecting trace amounts of swelling analytes mixed in nonswelling solvents. Using ethanol–hexane solutions as proof-of-concept mixtures, the ethanol detection limit of 150 ppm has been demonstrated. Besides reusable sensors, which can find important applications in environmental monitoring and petroleum process/product control, the programmable SMP photonic crystals possessing high mechanical strengths and all-room-temperature processability can provide vast opportunities in developing reconfigurable/rewritable nanooptical devices.

S.-Y. Leo, C. Xu, A. T. Xie, Prof. P. Jiang
Department of Chemical Engineering
University of Florida
Gainesville, FL 32611, USA
E-mail: pjiang@che.ufl.edu
Y. L. Ni, Y. F. Zhang, Prof. C. Taylor
Department of Mechanical and Aerospace Engineering
University of Florida
Gainesville, FL 32611, USA
Y. Q. Dai, Dr. P. X. Qi
Department of Chemistry
University of Florida
Gainesville, FL 32611, USA
Dr. V. Basile
ITIA-CNR
Industrial Technologies and Automation Institute
National Council of Research
Via Bassini, 15, Milano 20133, Italy
The ORCID identification number(s) for the author(s) of this article can be found under https://doi.org/10.1002/adfm.201703522.

DOI: 10.1002/adfm.201703522

1. Introduction

Photonic crystals are periodic dielectric structures with forbidden photonic band gaps (PBGs).[1–3] Photons with frequencies lying in the PBGs cannot propagate through the crystals, providing enormous opportunities in controlling the flow of light in miniature volumes for photonic information technology, such as next-generation all-optical integrated circuits.[1,4–8] Compared with traditional passive photonic crystals with fixed lattice constants and PBGs (or optical stop bands if the refractive index contrast of the artificial crystal is not high enough),[9–11] reconfigurable/rewritable photonic crystals with adjustable microstructures and PBGs could greatly expand the photonic functionalities and/or processability/manufacturability of integrated optical devices.[12–17] Smart shape memory polymers (SMPs), which can memorize and transit between a permanent shape and one or multiple temporary configurations in responding to various stimuli, such as heat, light, solvents, and electromagnetic fields,[18–25] may hold the key to truly reconfigurable photonic crystals. In sharp contrast to tunable photonic crystals enabled by stimuli-responsive elastic materials, like elastomers and gels,[26–33] the intermediate states of the reconfigurable photonic crystals are structurally fixed and they maintain the "frozen" photonic configurations even after releasing the programming driving forces (e.g., mechanical stress).

Thermoresponsive SMPs, which are activated by either direct or indirect (e.g., light absorption and alternating magnetic field) heating,[34–37] are mostly exploited. Shape memory efforts in these SMPs usually involve three steps including "hot" programming, room-temperature storage, and heat-triggered recovery. During "hot" programming, a SMP sample is first heated above a specific transition temperature (T_{trans}), such as its glass transition temperature (T_g), and then deformed from its permanent shape to a temporary geometry. After cooling below T_{trans}, the fixed temporary shape can be stored under ambient conditions for a long period of time. Recovery of the memorized permanent shape can finally be activated by reheating the sample above T_{trans} to leverage the entropy

elasticity of the stressed macromolecular chains.[19] Thermoresponsive SMPs have recently been utilized in fabricating smart, programmable nanooptical components, such as diffraction gratings and optical beam-power splitters.[38–44] However, heat-demanding SM programming and recovery steps greatly limit the broad applications of thermoresponsive SMPs in integrated nanooptical devices, including reconfigurable photonic crystals. In addition, the response speeds (for both programming and recovery steps) of thermoresponsive SMPs are controlled by the heat transfer rate through the bulky samples, though most polymers are not good heat conductors. This could significantly impede their optical applications in active devices (e.g., optical switches and displays), which typically require fast response speed.[45,46]

Novel SMPs that enable nontraditional, all-room-temperature shape memory (SM) cycles could facilitate to resolve the major drawbacks of thermoresponsive SMPs in developing active, programmable nanooptics. Room-temperature "cold" programming has been demonstrated for a variety of SMP systems, such as epoxies, polyurethanes, natural rubbers, polylactic acid-polyurethane blends, and copolymers comprising poly(ε-caprolactone) (PCL).[47–52] The convenient preparation of temporary shape is usually achieved by directly stretching or compressing the SMPs under ambient conditions through "reversible plasticity shape memory" or strain-induced polymer crystallization.[52,53] Unfortunately, heat-triggered recovery (including indirect photothermal effects induced by laser absorption)[34] is still needed for almost all "cold" programmable SMPs.[47] On the other hand, room-temperature SM recovery has also been achieved for SMPs like polyurethane, poly(vinyl alcohol), and polytriazole by exploring plasticizing effects induced by swelling of polymers by solvents and/or water.[54–58] However, most of the existing SMPs that enable "cold" recovery are still programmed at high temperature, and they usually suffer from slow recovery speed limited by the diffusion of solvent/water molecules into macromolecular chains. Up to date, SMPs exhibiting rapid all-room-temperature SM cycles are rare.[34,59]

We have developed a series of SMPs, which are copolymers of ethoxylated acrylates, to enable unconventional all-room-temperature SM effects.[60–62] Unfortunately, these hydrophilic copolymers with very low T_g (≈–40 °C) and Young's modulus (E < 10 MPa) are highly brittle and susceptible to water, impeding their applicability in durable nanooptics. Recently, a hydrophobic polyurethane-based SMP with higher T_g (≈32 °C) and E (≈150 MPa for a solid membrane and ≈41.7 MPa for a macroporous film) has been demonstrated to show mechanical compression-induced "cold" programming and room-temperature SM recovery triggered by various vapors and solvents.[59] Herein, by conducting extensive experimental and theoretical investigations on swelling-induced plasticizing effects during both SM programming and recovery steps, we have demonstrated reversible and reproducible all-room-temperature SM cycles using a new polyurethane-*co*-tripropylene glycol diacrylate (PU-*co*-TPGDA) copolymer with much improved thermomechanical/mechanical properties (T_g ≈87 °C, E ≈3 GPa for a solid membrane and ≈0.47 GPa for a macroporous copolymer). Most importantly, the fundamental insights gained in these mechanistic studies have resulted in the development of reusable chromogenic sensors for selectively detecting trace amounts of swelling analytes (e.g., ethanol) mixed in non-swelling solvents (like alkanes).

2. Results and Discussions

2.1. Unconventional All-Room-Temperature Shape Memory Cycle

The schematic illustration in **Figure 1** shows the unconventional all-room-temperature SM cycle enabled by the templated macroporous PU-*co*-TPGDA photonic crystal membranes. These self-standing SMP membranes are prepared by following the well-established colloidal templating approach using convectively self-assembled silica colloidal crystals as structural templates.[63] The Bragg diffraction of visible light from the periodic arrays of macropores leads to the striking iridescent colors of the macroporous membranes. The SMP sample in **Figure 2**a with a shining greenish color comprises periodic macropores templated from 290 nm silica microspheres. The cross-sectional scanning electron microscope (SEM) image in Figure 2b demonstrates the 3D highly ordered, inverted photonic crystal structure, which represents the permanent configuration of the SMP. It is interesting to notice that this permanent configuration can be "cold" programmed into stable temporary shapes by controlling the evaporation rates of various solvents (e.g., acetone, ethanol, and toluene) imbibed in the interconnecting macropores at ambient conditions. When the solvent in the macropores evaporates rapidly (<10 s), the SMP membrane maintains its original iridescent color (see Video S1 in the Supporting Information), which indicates the preservation of the permanent periodic photonic crystal structure. In sharp contrast, the shining greenish color of the same membrane changes to a dim bluish tone (Figure 2c) when the solvent evaporates slowly (>1 min) by covering the sample with a lid (see Video S2 in the Supporting Information). The cross-sectional SEM image in Figure 2d illustrates the collapse of the original periodic arrays of macropores after this slow solvent evaporation process. Additionally, the average thickness of the macroporous layer reduces from 2.49 ± 0.06 to 1.68 ± 0.11 μm. The SMP membrane with this temporary, disordered configuration can be stored at ambient conditions for a long period of time (at least 6 months). Surprisingly, the "frozen" temporary shape instantaneously recovers back to the memorized permanent configuration when the "cold" programmed sample is exposed to various solvent vapors, such as acetone and dichloromethane, at room temperature (see Video S3 in the Supporting Information), or immersed in liquid solvents, followed by fast solvent evaporation (see Video S4 in the Supporting Information). The full SM recovery of the shining greenish color and the original 3D periodic structure is evidently shown in Figure 2e,f. Besides cross-sectional SEM characterization, the changes in surface morphology and roughness during the room-temperature SM recovery process were further characterized by top-view SEM and atomic force microscope (AFM) images. The SEM images in Figure S1a,b in the Supporting Information compare the "cold" programmed and the acetone-vapor-recovered sample, respectively. Apparently,

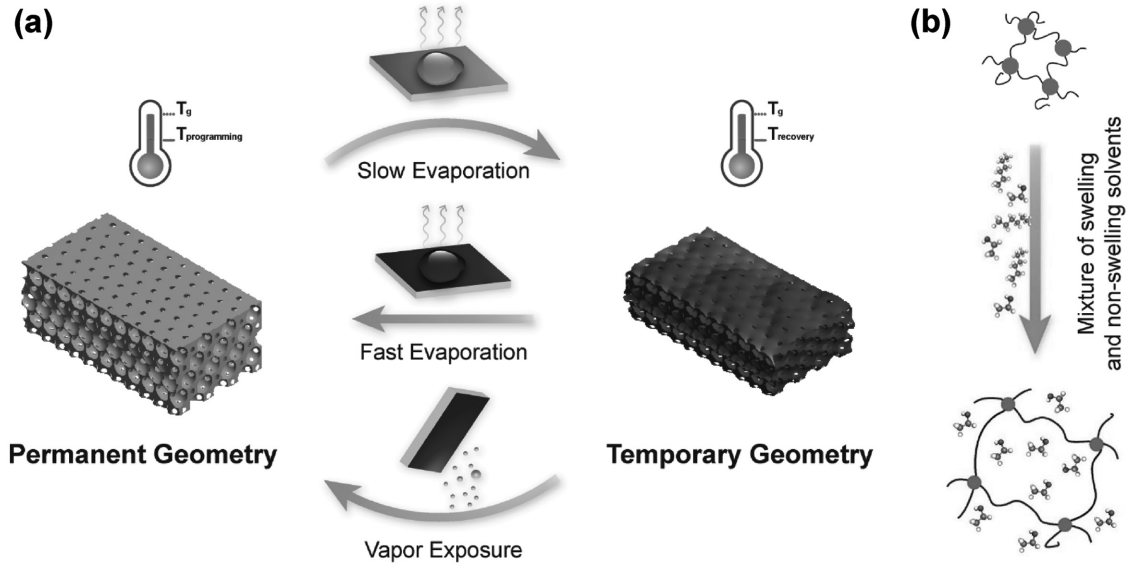

Figure 1. a) Schematic illustration showing the chromogenic and microstructural transitions between the permanent (3D highly ordered) and the temporary (disordered) configuration of a macroporous SMP membrane in an unconventional all-room-temperature SM cycle. The "cold" programming is induced by slow solvent evaporation; while the SM recovery is triggered by either vapor exposure or fast solvent evaporation. b) Schematic illustration showing the volume expansion of crosslinked polymer network caused by selective diffusion of swelling molecules (ethanol) in a mixture containing nonswelling hexane molecules.

the 2D long-range ordering of the templated macropores is retained on the membrane surface even for the deformed sample (Figure S1a, Supporting Information). The AFM scans in Figure S1c,d in the supporting information illustrate that the "cold" programmed sample with an average root mean square (RMS) roughness (R_q) of 14.9 ± 3.1 nm is rougher than that of the recovered membrane ($R_q \approx 7.4 \pm 0.9$ nm).

2.2. In Situ Optical Characterization of All-Room-Temperature SM Effects

Complementing standard SEM and AFM characterization, the striking chromogenic effects exhibited by the templated macroporous SMP photonic crystals provide a simple, sensitive, and noninvasive approach for in situly investigating nanoscopic SM effects during unconventional all-room-temperature SM cycles. **Figure 3** compares the normal-incidence optical reflection spectra obtained from a macroporous PU-*co*-TPGDA membrane with periodic 290 nm macropores, and the same sample after a slow and a fast solvent (acetone) evaporation process, respectively. Apparently, the spectrum of the fast-dried sample (blue curve) matches that of the original photonic crystal membrane (black curve). Both spectra show distinct optical stop bands near 530 nm and well-defined Fabry–Perot fringes. Additionally, these experimental spectra match reasonably well with the calculated reflection spectrum using a scalar-wave approximation (SWA) model,[64] which assumes a perfect face-centered cubic (FCC) crystalline lattice of 290 nm macropores. These optical experimental and modeling results demonstrate the preservation of the high crystalline quality of the original macroporous photonic crystal during the fast solvent evaporation process. By contrast, the slow-dried sample (red curve) only shows a broad peak centered around 440 nm, and its reflection amplitude (with a typical reflectance of ≈20%) is significantly smaller than that of the original or the fast-dried sample (with a typical reflectance of ≈80%). Moreover, the Fabry–Perot fringes, which originate from the interference between reflections from the ordered multilayers of the macroporous photonic crystal,[64] disappear in the spectrum of the slow-dried membrane. These optical reflection measurements correspond well with the dim bluish appearance and the collapse of the periodic microstructure perpendicular to the sample surface exhibited by the slow-dried membrane (see Figure 2c,d).

The in situ, noninvasive optical reflection measurements also enable the dynamic characterization of the changes in the photonic crystal properties during the slow and the fast solvent evaporation processes. **Figure 4**a,b shows 3D and 2D plots of color-coded, time-resolved normal-incidence optical reflection spectra continuously obtained from a macroporous SMP membrane during slow acetone evaporation. Due to the refractive index matching between acetone and the PU-*co*-TPGDA copolymer, the macroporous sample initially exhibits near-zero reflection when the macropores are filled up with liquid acetone. A stable, low-amplitude peak centered around 440 nm gradually appears when acetone slowly evaporates in ≈2 min from the membrane. In sharp contrast, the plots in Figure 4c,d show that strong Bragg diffraction peaks with distinct Fabry–Perot fringes emerge when acetone rapidly evaporates in ≈7 s from the sample, indicating the maintenance of the 3D ordered structure during this fast solvent evaporation process.

Besides acetone, a large variety of other solvents can also induce "cold" programming when they slowly evaporate from the macroporous SMP membranes under ambient conditions. The normal-incidence optical reflection spectra in Figure S2 in the Supporting Information show that some common

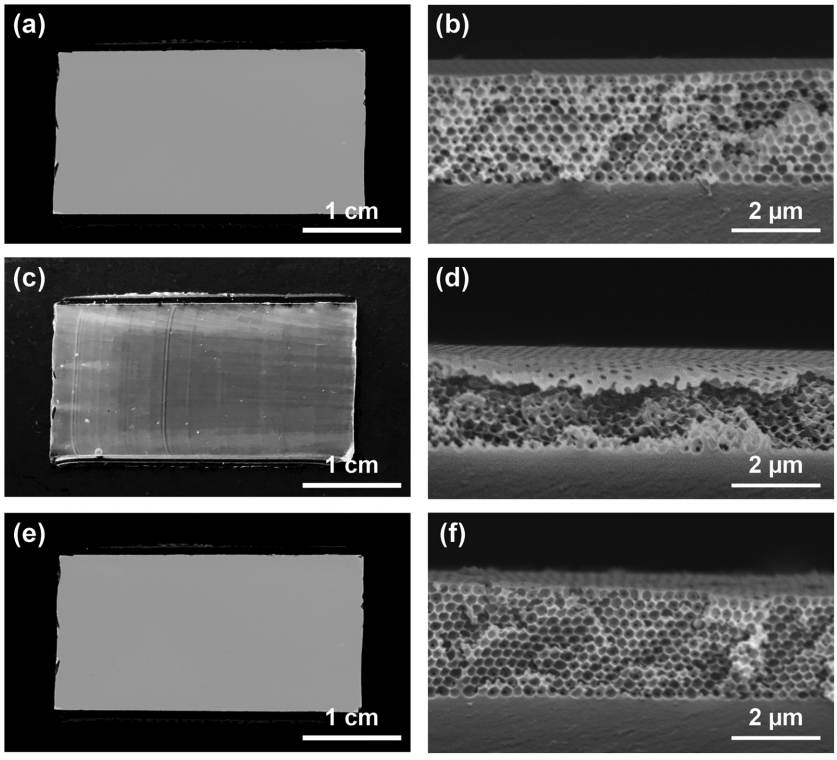

Figure 2. Photographs and typical cross-sectional SEM images showing the striking chromogenic and microstructural transitions during an all-room-temperature SM cycle of a macroporous SMP membrane comprising 290 nm macropores. a,b) Permanent configuration with 3D-ordered macropores. c,d) Temporary configuration with collapsed macropores induced by slow evaporation of liquid acetone. e,f) Recovered configuration triggered by exposing the deformed membrane to acetone vapor.

solvents, including acetonitrile, ethanol, benzene, and dichloromethane, can trigger significant spectral blue-shift, peak amplitude reduction, and Fabry–Perot fringe disappearance, similar to the effects exhibited by the slow evaporation of liquid acetone. Although the final dim colors of the deformed SMP membranes vary slightly (shown by the different diffraction peak positions), the spectra obtained from different programming run using a specific solvent overlap with each other quite well, indicating good reproducibility of this simple "cold" programming process (see Figure S3 in the Supporting Information). However, not all solvents can induce "cold" programming. The diffraction colors and the reflection spectra obtained after slowly evaporating liquid hexane and cyclohexane match those of the original SMP membranes (see Video S5 in the Supporting Information), revealing the maintenance of the permanent 3D-ordered structure.

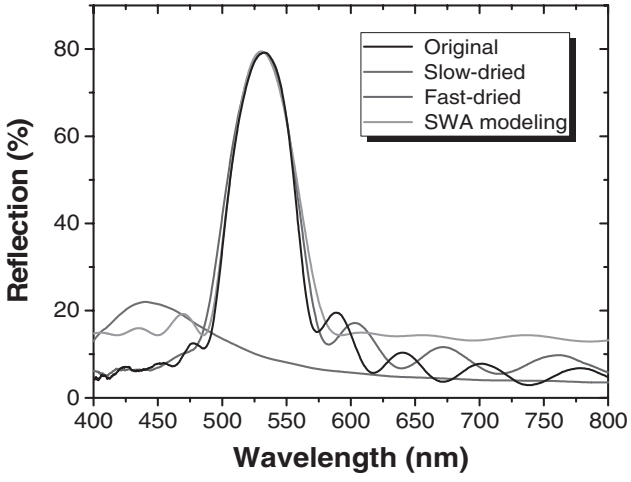

Figure 3. Normal-incidence optical reflection spectra obtained from a macroporous PU-*co*-TPGDA membrane comprising periodic 290 nm macropores, and the same sample after slow and fast acetone evaporation. The SWA-simulated spectrum is also shown to compare with the experimental spectra.

The room-temperature SM recovery of the memorized photonic crystal structure from the temporary, disordered configuration can also be readily characterized by the in situ optical technology. **Figure 5** compares the optical reflection spectra obtained from a "cold" programmed sample and the same sample after exposing to various solvent vapors. Apparently, all solvents that can "cold" program the SMP membranes, including acetone, acetonitrile, ethanol, benzene, and dichloromethane, also activate the recovery of the permanent configuration, which is confirmed by the reappearance of the strong Bragg diffraction peaks near 530 nm and the associated Fabry–Perot fringes. Besides their vapors, the liquid solvents can also trigger the same SM recovery if they rapidly evaporate from the SMP samples (<10 s). By contrast, both vapors and liquids of hexane and cyclohexane cannot stimulate the SM recovery as evidenced by the retainment of the dim blueish appearance and the weak reflection peaks centered around 440 nm. Figure S3 in the Supporting Information shows the absolute maximum amplitudes of the reflection peaks obtained from a macroporous SMP membrane cyclically deformed (by slow evaporation of liquid acetone) and then recovered by acetone vapor over 500 SM cycles. The high reproducibility in optical performance over cyclic all-room-temperature SM operations is clearly evident.

2.3. Underlying Mechanisms of Slow-Solvent-Evaporation-Induced "Cold" Programming

The unconventional "cold" programming is attributed to the synergistic effects of swelling-induced T_g reduction[54,57] and solvent-evaporation-stimulated capillary pressure.[61,65] The swelling ratios of the PU-*co*-TPGDA copolymer in various solvents, which are defined as: $\frac{W_{wet} - W_{dry}}{W_{dry}}$, where W_{wet} and W_{dry} are the weights of the samples measured after and prior to immersing in the solvents, are compared in **Figure 6**. Apparently, the solvents that enable "cold" programming, like acetonitrile, acetone, and ethanol, all swell the SMP membranes to different

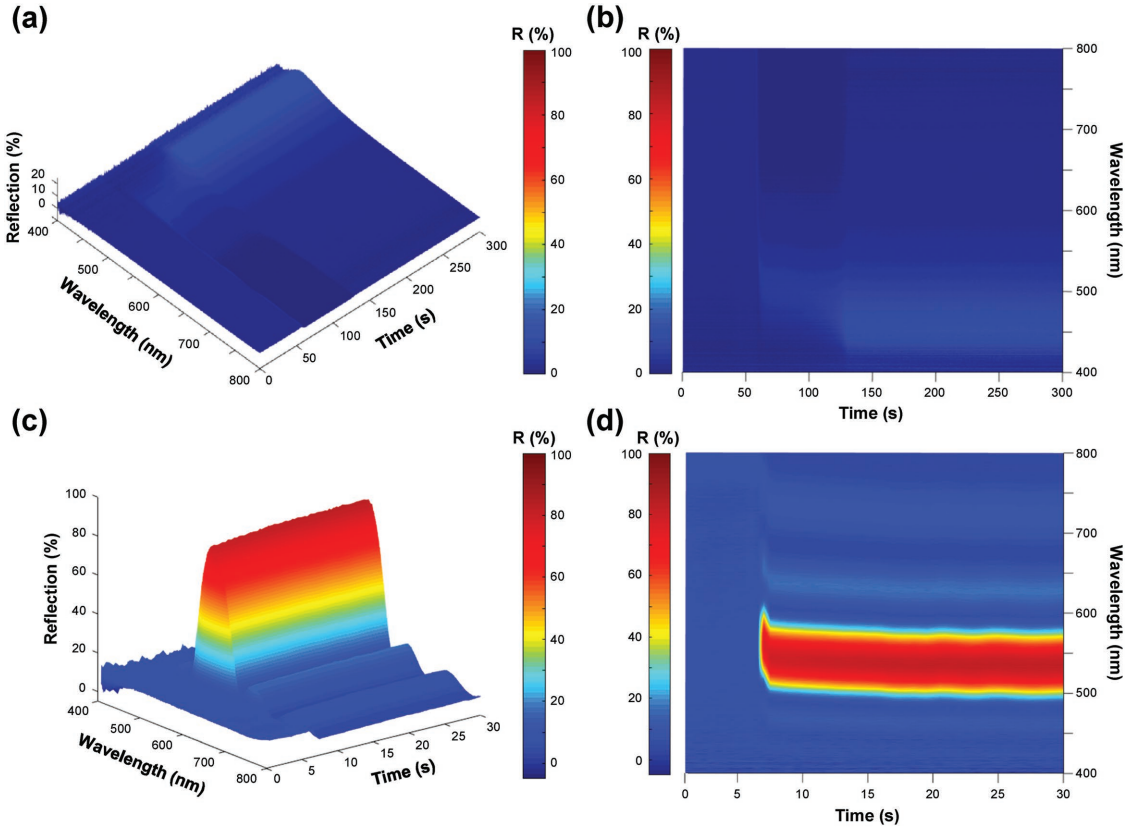

Figure 4. Color-coded, time-resolved 3D and 2D plots of normal-incidence optical reflection spectra continuously obtained from a macroporous SMP membrane comprising 290 nm macropores during slow (a,b) and fast (c,d) evaporation of acetone.

extents. In sharp contrast, all liquid alkanes and cycloalkanes (e.g., hexane and cyclohexane) cause negligible swelling even after long immersion time. The uptake and retention of the swelling solvents in the copolymer were qualitatively characterized by using Fourier transform infrared spectroscopy (FTIR). Figure S4 in the Supporting Information compares the FTIR spectra obtained from an original macroporous SMP membrane and the same sample after immersing in ethanol, acetonitrile, and acetone for 15 min, followed by air drying. The characteristic absorption bands corresponding to the hydroxyl (O—H), nitrile (C—N), and ketone (C=O) functional groups either strengthen (for ethanol and acetone-swollen samples) or emerge (for acetonitrile-swollen membrane), indicating the retention of the solvent molecules in between the crosslinked macromolecular network. The absorbed solvent molecules can function as plasticizers to significantly reduce the T_g and the Young's modulus of the SMP copolymer.[54,57] The typical differential scanning calorimetry (DSC) plots in **Figure 7** show that the T_g of the copolymer greatly reduces from ≈86.6 to ≈23.5 °C after immersing in acetone for 8 h. As the T_g of the solvent-swollen SMP is close to room temperature, the sample becomes very soft and flexible. The Young's moduli measured by nanoindentation tests (see a typical indentation force-displacement curve in Figure S5 in the Supporting Information) reduce greatly from 3.01 ± 0.12 GPa (solid copolymer membrane) and 0.47 ± 0.06 GPa (macroporous copolymer) to 4.2 ± 1.3 MPa (solid) and 1.1 ± 0.1 MPa (macroporous) for the acetone-swollen membranes. The solvent evaporation from the membrane surface could decrease the local temperature

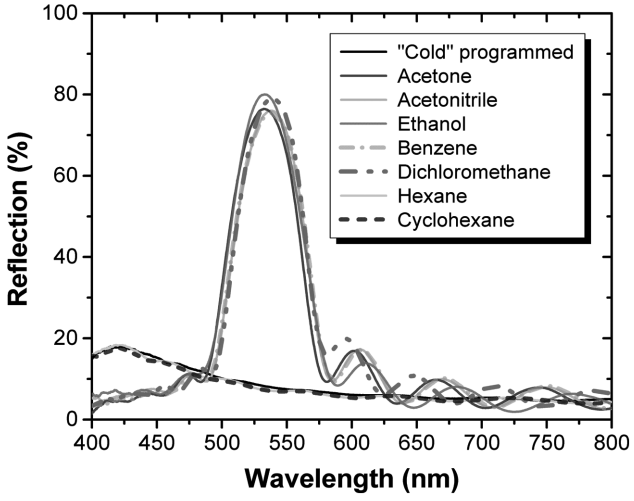

Figure 5. Normal-incidence optical reflection spectra obtained from a "cold" programmed SMP membrane prepared by slow evaporation of acetone, and the same sample after exposing to various solvent vapors at room temperature.

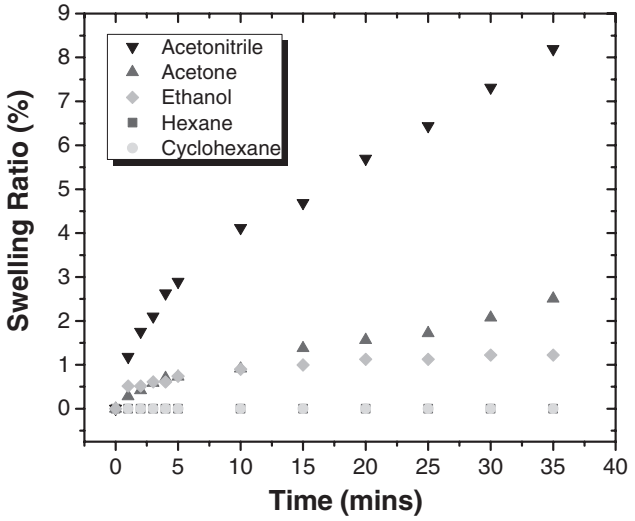

Figure 6. Swelling ratios of macroporous PU-*co*-TPGDA membranes in various solvents at different immersion durations.

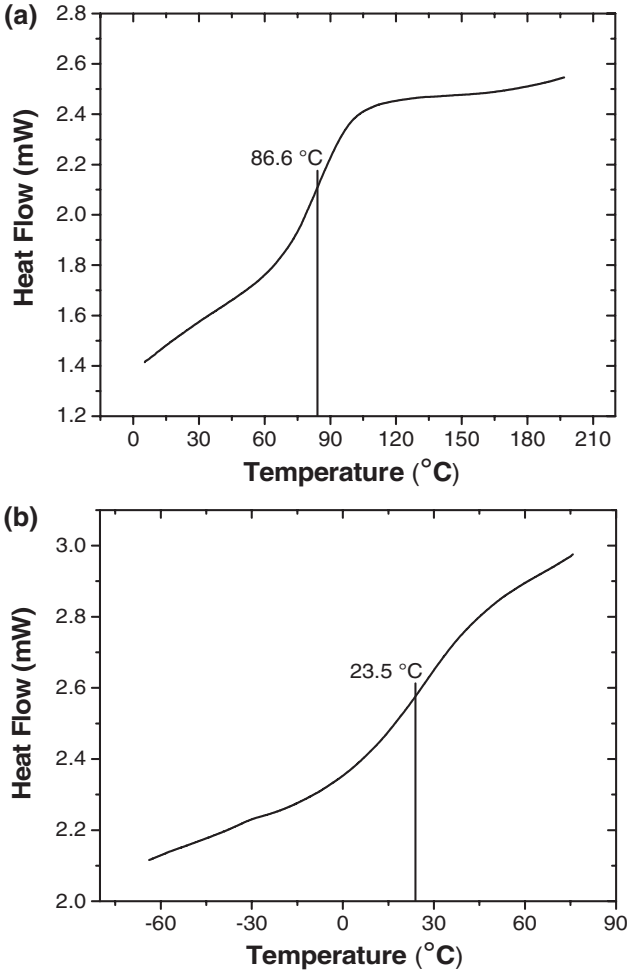

Figure 7. Typical DSC plots of a) an original macroporous PU-*co*-TPGDA membrane and b) the same sample after soaking in acetone for 8 h.

and thus affect the properties of the SMP and the liquid (e.g., surface tension). We measured the local temperature changes using an ennoLogic dual laser infrared thermometer caused by both slow and fast evaporation of one droplet of acetone on macroporous SMP membranes. The temperature dropped from ≈22.1 (room temperature) to ≈21.6 °C for fast drying and ≈20.4 °C for slow drying. As these temperature changes are quite small, we believe their effects will be limited.

Once the Young's modulus of the SMP is reduced to become comparable with the capillary pressure (P_c) generated by the solvent evaporation from the interconnecting macropores, the original 3D-ordered structure can be vertically deformed, resulting in the observed partial collapse of the macropores perpendicular to the substrate (Figure 2d) and the maintenance of the 2D periodic structure on the membrane surface (Figure S1a, Supporting Information). The capillary pressure can be calculated using the Young–Laplace equation as: $P_c = 2\gamma\cos\theta/r$, where γ is the liquid/vapor surface tension, θ is the contact angle of the solvent on the copolymer surface, and r is the radius of the air cavity in the center of the solvent droplet confined by the SMP macropore.[65] For liquid acetone with $\gamma = 25.2$ mN m^{-1} and $\cos\theta \approx 1$ (as acetone wets the copolymer), the minimum P_c, which occurs at the end of the evaporation process (i.e., when r reaches the maximum and equals the radius of the macropores), is calculated to be ≈0.35 MPa. Higher P_c triggered at the beginning stage of the droplet evaporation from the macropores can easily surpass the reduced Young's modulus of the solvent-swollen copolymer, leading to the temporary, deformed configuration of the macropores. Van der Waals attractions between the stressed macromolecular chains can then stabilize the deformed macropores after the vanishing of P_c caused by the complete evaporation of the solvent. Similar capillary pressure-induced macropore collapse has been extensively investigated as it underlies a broad spectrum of technologies ranging from polymer reverse osmosis membranes for advanced water purification to enhanced oil recovery in petroleum reservoirs.[66,67]

To gain fundamental insights into the effects of the solvent evaporation rate on the unconventional "cold" programming process, we modeled the copolymer swelling process as a simplified 1D solvent diffusion problem using Fick's second law. The diffusion coefficient (D) of a solvent in the copolymer membrane, which is assumed to be an infinite slab with thickness l, is determined using a numerical model describing the fractional mass uptake of the solvent by the SMP as: $\frac{M_t}{M_\infty} = 1 - \sum_{n=0}^{\infty} \frac{8}{(2n+1)^2\pi^2} \exp\{-D(2n+1)^2\pi^2 t/4l^2\}$, where M_t and M_∞ denote the mass uptake at time t and ∞, respectively.[68] **Figure 8**a shows the calculated diffusion coefficients at different durations for liquid acetone using the corresponding swelling ratio data in Figure 6. The average diffusion coefficient is determined to be ≈2.33×10^{-8} cm^2 s^{-1}, which agrees well with the values reported in previous work studying the diffusion of acetone in SM polyurethane films.[69] Using this diffusion coefficient, we then modeled the dependence of the transient fractional mass uptake versus the diffusion time and length (Figure 8b). As the topmost macroporous layer dominates the capillary pressure-induced "cold" programming process, we only need to consider the diffusion of acetone in this

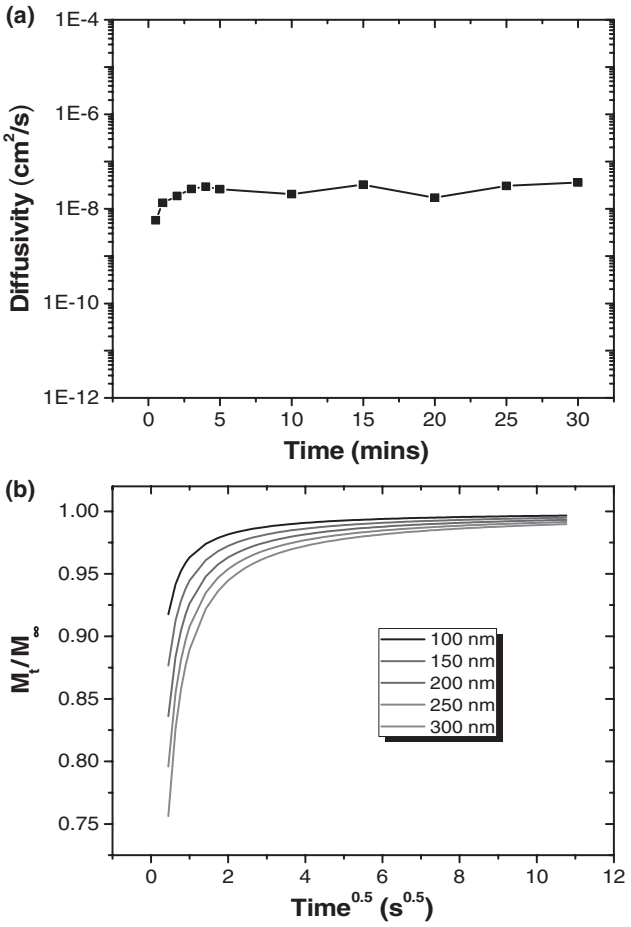

Figure 8. a) Calculated transient diffusivities of acetone in PU-*co*-TPGDA copolymer. b) Modeled dependence of transient fractional mass uptake of acetone by the copolymer versus diffusion time and length using Fick's second law.

microscopic layer comprising interconnecting macropores. The cross-sectional SEM image in Figure 2b indicates that the copolymer wall thickness between the close-packed macropores is smaller than the radius of the macropores. The Fickian plot in Figure 8b illustrates that it will only take a few seconds to reach the near-saturation absorption of acetone in the copolymer walls with thickness ranging from 100 to 300 nm. In our model, the complex macroporous geometry, which will significantly complicate the transport calculations, has not been taken into account in the transport calculations for the following reasons. First, the templated SMP macropores are highly interconnected and can be completely wetted by the solvents used in this study. Therefore, the thin macroporous layer can be momentarily filled up by the solvents. Second, as the length scale of interest is only nanoscopic, the effects of the curvature/geometry of the macropores on the dynamics of solvent diffusion will be diminished.

Although our modeling results show that the solvent diffusion in thin macroporous walls is fast, the relaxation of the polymer chains due to solvation plays a crucial role in determining the dynamics of the drastic reduction in T_g and the Young's modulus of the SMP copolymer.[70] Previous studies have revealed that the kinetics of the solvent-swelling-induced plasticizing effect is mainly determined by the rate of the polymer chain relaxation, rather than the diffusion of small solvent molecules into the polymer network.[70] Detailed kinetic dynamic mechanical analysis (DMA) experiments using polyurethane-based SMP foams have demonstrated that it takes ≈1 min for the storage moduli of the macroporous SMPs to be significantly reduced after immersing in various solvents (e.g., ethanol).[69] Based on these facts, the effects of the solvent evaporation rate on the unusual "cold" programming process can be explained as follows. For slow evaporation (>1 min), the polymer chains can be sufficiently relaxed by the absorbed solvent molecules,[71] leading to the much reduced Young's modulus. The large capillary pressure created by solvent evaporation can then deform the softened macropores. By contrast, during fast solvent evaporation, the glassy SMP retains its high modulus which exceeds P_c, resulting in the preservation of the original photonic crystal structure and the corresponding diffraction color.

2.4. Mechanisms of Swelling-Induced SM Recovery

Similar to traditional thermoresponsive SMPs, we believe the entropy elasticity underlies the room-temperature SM recovery triggered by various swelling vapors and liquids. This claim is supported by two straightforward evidences. First, as shown in Figure S6a in the Supporting Information, the "cold" programmed SMP can be thermally recovered back to the permanent configuration only when the sample is heated above the T_g of the copolymer. The optical reflection spectrum of the thermally activated membrane matches the spectra of the samples recovered by different swelling solvents. Second, as demonstrated in our previous work,[42] macroporous PU-*co*-TPGDA membranes can be "hot" programmed by applying a high clamp pressure at temperature above T_g. The periodic photonic crystal structure is completely distorted in this process, leading to a nearly flat optical reflection curve (Figure S6b, Supporting Information). Importantly, the spectra in Figure S6b in the Supporting Information show that the full SM recovery can be achieved by exposing the "hot" programmed samples to the vapors of acetone, acetonitrile, ethanol, and dichloromethane under ambient conditions; while no recovery is observed for nonswelling hexane and cyclohexane vapors.

We believe the diffusion of small solvent molecules and the swelling of the copolymer also dominate the room-temperature SM recovery. In the vapor-triggered recovery process, as demonstrated in our previous work, the solvent molecules in the vapor phase first condense in the interconnecting macropores through capillary condensation.[60] The condensed liquid then rapidly diffuses into the polymer network and expands the deformed macroporous layer. This volume expansion weakens the Van der Waals interactions between the stressed macromolecular chains, triggering the instantaneous SM recovery.[54] Critically, the polymer still retains its high Young's modulus in this rapid diffusion process which surpasses P_c created by the subsequent fast evaporation of the swelling solvent from the macropores. The same mechanism can also explain the recovery of the periodic photonic crystal structure by immersing

the deformed SMP membranes in swelling liquids, followed by rapid solvent evaporation.

2.5. Chromogenic Sensing of Ethanol in Hexane Using Macroporous SMP Membranes

The above fundamental investigations have revealed that many swelling solvents can trigger SM recovery of "cold" and "hot programmed macroporous SMP membranes, leading to striking color changes that can be easily distinguished by naked eyes. By contrast, all liquid alkanes and cycloalkanes show negligible swelling of the SMP copolymer and no chromogenic effects. Therefore, we speculate that the macroporous SMPs can be used as chromogenic sensors for selectively detecting a swelling agent mixed in a nonswelling solvent. Here, we used ethanol–hexane mixtures as proof-of-concept examples to demonstrate the capabilities of these novel chemical sensors. This solution system is technologically important as ethanol has been worldwide blended with gasoline (a mixture of alkanes, cycloalkanes, and olefins) to make fuels consumed in motor vehicles with gasoline engines. However, ethanol can severely damage the rubber and aluminum components of traditional fuel systems and gasoline engines, especially for aircraft fuel systems. Ethanol fuel sensing is thus frequently conducted by pilots and other people that require ethanol free gasoline. **Figure 9**a compares the optical reflection spectra obtained from a "cold" programmed macroporous SMP membrane with 290 nm macropores, and the same sample after immersing in 10 mL ethanol–hexane solutions with different ethanol concentrations (from 10 vol% to 700 ppm) for 3 s, followed by fast solvent evaporation. Apparently, the mixture with a high ethanol content (10 vol%) can rapidly swell the deformed macropores, leading to a full SM recovery. Importantly, lower concentrations of ethanol slow the diffusion dynamics and affect the extents of the final swelling-induced SM recovery, resulting in easily perceived color changes as evidenced by the different diffraction peak positions and amplitudes. The sensitivity of these chromogenic sensors can be further improved by extending the immersion duration (i.e., diffusion time) of the macroporous samples in solutions with even lower ethanol concentrations. Figure 9b shows that 150 ppm ethanol can trigger a distinct partial recovery of the "cold" programmed macropores after immersing in the solution for 2 h. Although here we only show the results for selectively sensing ethanol in hexane, our preliminary experiments demonstrate that the concept can be easily extended to detecting ethanol in other alkanes (e.g., octane) and even gasoline.

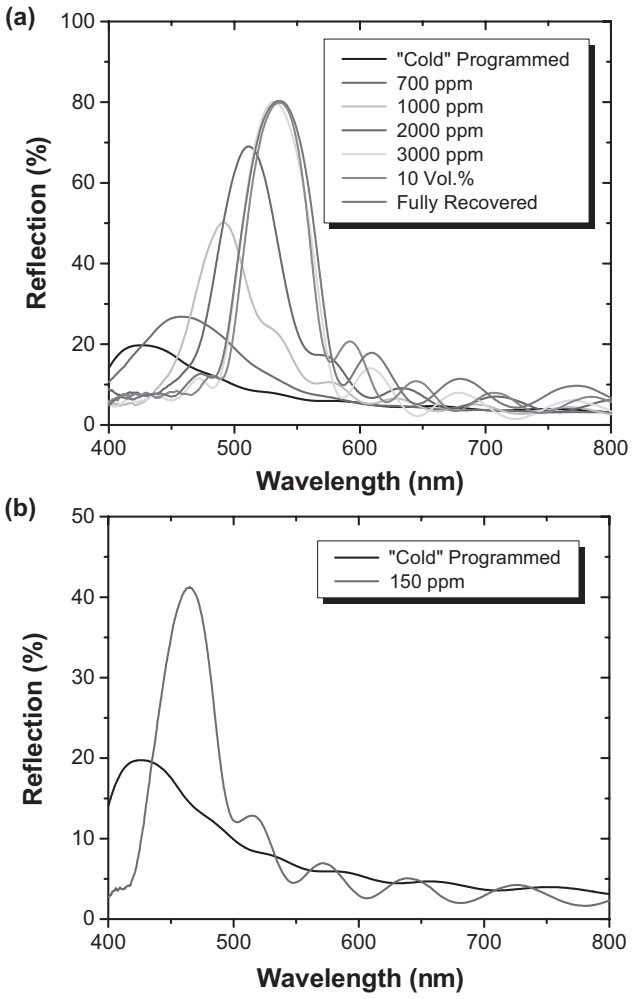

Figure 9. Chromogenic sensing of ethanol in hexane using a macroporous PU-*co*-TPGDA membrane comprising 290 nm macropores. a) Dipping in solutions with different ethanol concentrations for 3 s. b) Soaking in 150 ppm solution for 2 h.

3. Conclusion

In conclusion, we have demonstrated unconventional, all-room-temperature SM programming and recovery of macroporous PU-*co*-TPGDA copolymer with a high T_g (≈87 °C) by simply controlling the evaporation rates of various swelling solvents. Our experimental and theoretical investigations reveal that polymer swelling caused by the diffusion of small solvent molecules in the crosslinked macromolecular network dominates both processes. In slow-evaporation-induced "cold" programming, large capillary pressure created by solvent evaporation from the interconnected macropores surpasses the significantly reduced Young's modulus of the solvent-swollen SMP, leading to the collapse of the original, periodic photonic crystal structure. Similarly, rapid diffusion of solvent molecules in the deformed polymer chains triggers instantaneous SM recovery of the macropores with nanoscopic wall thickness. Importantly, we find that the PU-*co*-TPGDA copolymer exhibits negligible swelling by alkanes (both cyclic and acyclic). By using ethanol–hexane solution as an exemplary system, we have demonstrated the selective sensing of trace amounts of ethanol in hexane with a detection limit of 150 ppm by monitoring the apparent color changes associated with the swelling-induced SM recovery. These SMP-enabled chromogenic sensors could find many important technological applications ranging from environmental monitoring (e.g., detecting trace amounts of benzene/toluene/xylene (BTX) in polluted water) to petroleum process/product control. Our preliminary results show that a

detection limit of ≈500 ppm for BTX in water can be readily achieved using the SMP photonic crystal sensors. Additionally, by further exploring the compositions and differential swelling properties of many available SMPs, we believe the concept can be applied to detecting trace amounts of analytes in a spectrum of solution and/or vapor mixture systems.

4. Experimental Section

Materials, Instrumentation, and Sample Characterization: All solvents and chemicals were of reagent quality and were used without further purification. Monodispersed silica microspheres with 290 nm diameter and less than 5% diameter standard deviation were synthesized by the standard Stöber method.[72] They were purified by multiple centrifugation and redispersion cycles (at least 4 times) with 200-proof ethanol (Decon Labs). The commercial oligomer mixture (CN945A70), which is an aliphatic polyester/polyether-based trifunctional urethane acrylate oligomer (75 wt%) blended with tripropylene glycol diacrylate (25 wt%), was obtained from Sartomer. The photoinitiator, Darocur 1173 (2-hydroxy-2-methyl-1-phenyl-1-propanone), was provided by BASF. Hydrofluoric acid (49% aqueous solution) was purchased from Fisher Scientific.

A pulsed ultraviolet curing system (RC 742, Xenon) was utilized in photocuring the commercial oligomer mixture. A manual hydraulic press (Carver Model C) with a typical clamp force of 200 lb was used in "hot" programming macroporous SMP membranes. Scanning electron microscopy was carried out on a FEI Nova NanoSEM 430 unit. A thin layer of gold (5 nm) was sputtered onto the samples prior to imaging. Amplitude-modulation atomic force microscopy was conducted on a MFP-3D AFM (Asylum Research, Inc.) with a Nanosensor PPP-NCHR probe (tip radius < 10 nm). Nanoindentation tests were carried out on a Hysitron BioSoft Indenter. Differential scanning calorimetry thermograms were obtained using a Q1000 unit from TA Instruments at a heating rate of 10 °C min^{-1} and an empty pan as reference. FTIR spectroscopy was performed on a Thermo Nicolet 5700 spectrometer with a single bounce, diamond-stage attenuated total reflectance accessory. All spectra were collected at an average of 32 scans and 1 cm^{-1} resolution. Normal-incidence optical reflection spectra were gathered using an Ocean Optics HR4000 high-resolution vis-NIR spectrometer with a reflection probe (R600-7) and a tungsten halogen light source (LS-1). Absolute reflectivity was obtained as the ratio of the sample spectrum and a reference spectrum, which was the optical density obtained from an aluminum-coated (1000 nm thick) silicon wafer. The swelling ratios of the macroporous PU-*co*-TPGDA membranes in various swelling and nonswelling solvents were evaluated by measuring the mass increase after soaking in these solvents for different durations.

Templating Fabrication of Macroporous PU-co-TPGDA Photonic Crystal Membranes: The convective self-assembly technology was used in assembling silica microspheres into 3D highly ordered colloidal crystals on glass substrates.[63] The typical colloidal crystal thickness was ≈2.5 μm or ≈11 colloidal monolayers. Due to its relatively high viscosity (≈2200 cps at 60 °C), the commercial CN945A70 oligomer mixture was preheated to 90 °C before infiltrating into the interstitials of the close-packed silica colloidal crystals. The oligomers were then photopolymerized using the pulsed UV curing system for 4 s. After selectively dissolving the templating silica microspheres in a 2 vol% hydrofluoric acid aqueous solution, the templated macroporous SMP photonic crystals were rinsed with deionized water and finally dried in a stream of compressed air. This resulted in self-standing SMP membranes with a typical thickness of ≈1 mm, which was controlled by using a thick adhesive tape as a spacer in the above templating procedures.

"Cold" and "Hot" Programming of Macroporous SMP Membranes: For "cold" programming, a few drops of a swelling solvent (e.g., acetone) were added on the surface of a macroporous SMP membrane. As the interconnecting macropores were filled up with the refractive-index-matching fluid, the membrane became nearly transparent. A glass (or plastic) petri dish was then used to cover the sample to slow down the solvent evaporation rate. After the solvent was completely evaporated in 1–2 min, the resulting "cold" programmed membrane changed color from shining green to dim blue. For "hot" programming, a clamp force of 200 lb was applied on a macroporous SMP membrane using the Carver Model C hydraulic press at 90 °C for 3 min. The sample was then cooled down to room temperature with the clamp force still applied. After releasing the clamp force, the final membrane became transparent as the ordered macropores were fully deformed.

Shape Memory Recovery of "Cold" and "Hot" Programmed SMP Membranes: The "cold" or "hot" programmed SMP sample with deformed macropores was placed at ≈1 cm above the surface of a swelling solvent contained in a centrifuge tube for ≈3 s. After removing the sample from the vapor, the rapid evaporation (in a few seconds) of the condensed liquid in the interconnecting macropores led to the full SM recovery of the shining greenish color of the original SMP membranes. The room-temperature SM recovery could also be triggered by immersing the programmed sample in a liquid swelling solvent, followed by removing excess solvent using Kimwipes and then dried in compressed air. For testing heat-activated SM recovery, the "cold" programmed membranes were placed in an oven preset at different temperatures (from 50 to 90 °C) for 3 min. The samples were then removed from the oven and cooled down to room temperature.

Chromogenic Sensing of Ethanol in Hexane: The "cold" programmed SMP membranes were dipped in ethanol–hexane solutions with different concentrations ranging from 700 ppm to 10 vol% for 3 s at room temperature. The samples were then rapidly blow-dried using compressed air. For 150 ppm solution, the immersion duration was extended to 2 h to ensure sufficient diffusion of ethanol to the SMP sample. Optical reflection spectra of the ethanol-swollen SMPs were then measured to evaluate the ethanol contents in the mixtures.

Scalar Wave Approximation Optical Modeling: The scalar wave theory developed for modeling the diffractive properties of periodic dielectric structures[64] was used in simulating the normal-incidence reflection spectra from macroporous SMP photonic crystals. In this method, Maxwell's equations were solved for a periodic dielectric medium by considering diffraction from only one set of crystalline planes (e.g., (111) planes in the current case). The size of the macropores and the photonic crystal thickness used in the SWA modeling were determined by SEM characterization. A refractive index of 1.46 for the PU-*co*-TPGDA copolymer was used in the SWA calculations.

Supporting Information

Supporting Information is available from the Wiley Online Library or from the author.

Acknowledgements

This work was partially supported by the US Defense Threat Reduction Agency, Basic Research Award # HDTRA1-15-1-0022, to University of Florida and the US National Science Foundation (NSF) under Award No. CMMI-1562861. Acknowledgments were also made to the Florida Space Institute's Space Research Initiative Program (OR-DRPD-SRI2015) and Marie Curie IRSES Project247614-NET4m.

Conflict of Interest

The authors declare no conflict of interest.

Keywords

chromogenic sensors, cold programming, photonic crystals, sensors, shape memory polymers

Received: June 27, 2017
Revised: July 28, 2017
Published online: September 8, 2017

[1] J. D. Joannopoulos, R. D. Meade, J. N. Winn, *Photonic Crystals: Molding the Flow of Light*, Princeton University Press, Princeton, NJ **1995**.
[2] A. I. Kuznetsov, A. E. Miroshnichenko, M. L. Brongersma, Y. S. Kivshar, B. Luk'yanchuk, *Science* **2016**, *354*, 846.
[3] J. H. Moon, S. Yang, *Chem. Rev.* **2010**, *110*, 547.
[4] S. Y. Lin, E. Chow, V. Hietala, P. R. Villeneuve, J. D. Joannopoulos, *Science* **1998**, *282*, 274.
[5] C. Grillet, C. Monat, C. L. Smith, M. W. Lee, S. Tomljenovic-Hanic, C. Karnutsch, B. J. Eggleton, *Laser Photonics Rev.* **2010**, *4*, 192.
[6] S. F. Wu, S. Buckley, J. R. Schaibley, L. F. Feng, J. Q. Yan, D. G. Mandrus, F. Hatami, W. Yao, J. Vuckovic, A. Majumdar, X. D. Xu, *Nature* **2015**, *520*, 69.
[7] L. Wang, Q. Li, *Adv. Funct. Mater.* **2016**, *26*, 10.
[8] B. M. Boyle, T. A. French, R. M. Pearson, B. G. McCarthy, G. M. Miyake, *ACS Nano* **2017**, *11*, 3052.
[9] O. D. Velev, S. Gupta, *Adv. Mater.* **2009**, *21*, 1897.
[10] C. I. Aguirre, E. Reguera, A. Stein, *Adv. Funct. Mater.* **2010**, *20*, 2565.
[11] A. C. Arsenault, T. J. Clark, G. Von Freymann, L. Cademartiri, R. Sapienza, J. Bertolotti, E. Vekris, S. Wong, V. Kitaev, I. Manners, R. Z. Wang, S. John, D. Wiersma, G. A. Ozin, *Nat. Mater.* **2006**, *5*, 179.
[12] C. J. Zhang, G. G. Cano, P. V. Braun, *Adv. Mater.* **2014**, *26*, 5678.
[13] A. C. Bedoya, P. Domachuk, C. Grillet, C. Monat, E. C. Maegi, E. Li, B. J. Eggleton, *Opt. Express* **2012**, *20*, 11046.
[14] P. B. Deotare, I. Bulu, I. W. Frank, Q. M. Quan, Y. N. Zhang, R. Ilic, M. Loncar, *Nat. Commun.* **2012**, *3*, 846.
[15] D. P. Yang, Y. H. Qin, S. Y. Ye, J. P. Ge, *Adv. Funct. Mater.* **2014**, *24*, 817.
[16] Y. Montelongo, A. K. Yetisen, H. Butt, S. H. Yun, *Nat. Commun.* **2016**, *7*, 12002.
[17] W. B. Niu, L. C. Qu, R. W. Lyv, S. F. Zhang, *RSC Adv.* **2017**, *7*, 22461.
[18] C. Lowenberg, M. Balk, C. Wischke, M. Behl, A. Lendlein, *Acc. Chem. Res.* **2017**, *50*, 723.
[19] *Shape Memory Polymers* (Ed: A. Lendlein), Springer, New York, NY **2010**.
[20] Q. Zhao, W. K. Zou, Y. W. Luo, T. Xie, *Sci. Adv.* **2016**, *2*, e1501297.
[21] W. M. Huang, B. Yang, Y. Q. Fu, *Polyurethane Shape Memory Polymers*, CRC Press, Boca Raton, FL **2012**.
[22] Q. Zhao, H. J. Qi, T. Xie, *Prog. Polym. Sci.* **2015**, *49–50*, 79.
[23] T. Lv, Z. Cheng, D. Zhang, E. Zhang, Q. Zhao, Y. Liu, L. Jiang, *ACS Nano* **2016**, *10*, 9379.
[24] P. T. Mather, X. Luo, I. A. Rousseau, *Annu. Rev. Mater. Res.* **2009**, *39*, 445.
[25] H. Meng, H. Mohamadian, M. Stubblefield, D. Jerro, S. Ibekwe, S.-S. Pang, G. Li, *Smart Mater. Struct.* **2013**, *22*, 093001.
[26] Q. Q. Fu, B. T. Zhu, J. P. Ge, *Nanoscale* **2017**, *9*, 2457.
[27] M. S. Wang, Y. D. Yin, *J. Am. Chem. Soc.* **2016**, *138*, 6315.
[28] H. Fudouzi, Y. N. Xia, *Langmuir* **2003**, *19*, 9653.
[29] D. P. Yang, S. Y. Ye, J. P. Ge, *J. Am. Chem. Soc.* **2013**, *135*, 18370.
[30] J. Zhang, S. S. He, L. M. Liu, G. Z. Guan, X. Lu, X. M. Sun, H. S. Peng, *J. Mater. Chem. C* **2016**, *4*, 2127.
[31] Y. F. Yue, M. A. Haque, T. Kurokawa, T. Nakajima, J. P. Gong, *Adv. Mater.* **2013**, *25*, 3106.
[32] E. Lee, S. Yang, *MRS Commun.* **2015**, *5*, 97.
[33] Y. Kang, J. J. Walish, T. Gorishnyy, E. L. Thomas, *Nat. Mater.* **2007**, *6*, 957.
[34] G. Li, H. Zhang, D. Fortin, W. Z. Fan, H. S. Xia, Y. Zhao, *J. Mater. Chem. C* **2016**, *4*, 5932.
[35] H. Zhang, Y. Zhao, *ACS Appl. Mater. Interfaces* **2013**, *5*, 13069.
[36] H. Koerner, G. Price, N. A. Pearce, M. Alexander, R. A. Vaia, *Nat. Mater.* **2004**, *3*, 115.
[37] C. S. Hazelton, S. C. Arzberger, M. S. Lake, N. A. Munshi, *J. Adv. Mater.* **2007**, *39*, 35.
[38] C. A. Tippets, Q. Li, Y. Fu, E. U. Donev, J. Zhou, S. A. Turner, A.-M. S. Jackson, V. S. Ashby, S. S. Sheiko, R. Lopez, *ACS Appl. Mater. Interfaces* **2015**, *7*, 14288.
[39] S. Schauer, T. Meier, M. Reinhard, M. Rohrig, M. Schneider, M. Heilig, A. Kolew, M. Worgull, H. Holscher, *ACS Appl. Mater. Interfaces* **2016**, *8*, 9423.
[40] C. G. Schaefer, C. Lederle, K. Zentel, B. Stuehn, M. Gallei, *Macromol. Rapid Commun.* **2014**, *35*, 1852.
[41] H. Xu, C. Yu, S. Wang, V. Malyarchuk, T. Xie, J. A. Rogers, *Adv. Funct. Mater.* **2013**, *23*, 3299.
[42] Y. Fang, S. Y. Leo, Y. L. Ni, L. Yu, P. X. Qi, B. C. Wang, V. Basile, C. Taylor, P. Jiang, *Adv. Opt. Mater.* **2015**, *3*, 1509.
[43] A. Espinha, M. Concepcion Serrano, A. Blanco, C. Lopez, *Adv. Opt. Mater.* **2014**, *2*, 516.
[44] P. Li, Y. Han, W. X. Wang, Y. J. Liu, P. Jin, J. S. Leng, *Sci. Rep.* **2017**, *7*, 44333.
[45] S. Valkama, H. Kosonen, J. Ruokolainen, T. Haatainen, M. Torkkeli, R. Serimaa, G. Ten Brinke, O. Ikkala, *Nat. Mater.* **2004**, *3*, 872.
[46] A. C. Arsenault, D. P. Puzzo, I. Manners, G. A. Ozin, *Nat. Photonics* **2007**, *1*, 468.
[47] G. Q. Li, A. Q. Wang, *J. Polym. Sci., Part B: Polym. Phys.* **2016**, *54*, 1319.
[48] Y. Q. Mao, J. M. Robertson, X. M. Mu, P. T. Mather, H. J. Qi, *J. Mech. Phys. Solids* **2015**, *85*, 219.
[49] X. L. Wu, S. F. Kang, X. J. Xu, F. Xiao, X. L. Ge, *J. Appl. Polym. Sci.* **2014**, *131*, 40559.
[50] C. M. Yakacki, T. D. Nguyen, R. Likos, R. Lamell, D. Guigou, K. Gall, *Polymer* **2011**, *52*, 4947.
[51] B. Heuwers, A. Beckel, A. Krieger, F. Katzenberg, J. C. Tiller, *Macromol. Chem. Phys.* **2013**, *214*, 912.
[52] P. Ping, W. S. Wang, X. S. Chen, X. B. Jing, *Biomacromolecules* **2005**, *6*, 587.
[53] G. Q. Li, W. Xu, *J. Mech. Phys. Solids* **2011**, *59*, 1231.
[54] H. Du, J. Zhang, *Soft Matter* **2010**, *6*, 3370.
[55] E. Zharinova, M. Heuchel, T. Weigel, D. Gerber, K. Kratz, A. Lendlein, *Polymers* **2016**, *8*, 412.
[56] H. Kuroki, C. Islam, I. Tokarev, H. Hu, G. Liu, S. Minko, *ACS Appl. Mater. Interfaces* **2015**, *7*, 10401.
[57] W. M. Huang, B. Yang, L. An, C. Li, Y. S. Chan, *Appl. Phys. Lett.* **2005**, *86*, 114105.
[58] M. R. Ramdas, K. S. S. Kumar, C. P. R. Nair, *RSC Adv.* **2016**, *6*, 53602.
[59] Y. Fang, S. Y. Leo, Y. L. Ni, J. Y. Wang, B. C. Wang, L. Yu, Z. Dong, Y. Q. Dai, V. Basile, C. Taylor, P. Jiang, *ACS Appl. Mater. Interfaces* **2017**, *9*, 5457.
[60] Y. Fang, Y. L. Ni, B. Choi, S. Y. Leo, J. Gao, B. Ge, C. Taylor, V. Basile, P. Jiang, *Adv. Mater.* **2015**, *27*, 3696.
[61] Y. Fang, Y. L. Ni, S. Y. Leo, C. Taylor, V. Basile, P. Jiang, *Nat. Commun.* **2015**, *6*, 7416.
[62] Y. Fang, Y. L. Ni, S. Y. Leo, B. C. Wang, V. Basile, C. Taylor, P. Jiang, *ACS Appl. Mater. Interfaces* **2015**, *7*, 23650.

[63] P. Jiang, J. F. Bertone, K. S. Hwang, V. L. Colvin, *Chem. Mater.* **1999**, *11*, 2132.
[64] D. M. Mittleman, J. F. Bertone, P. Jiang, K. S. Hwang, V. L. Colvin, *J. Chem. Phys.* **1999**, *111*, 345.
[65] S. J. Gregg, K. S. W. Sing, *Adsorption, Surface Area and Porosity*, Academic Press Inc., London **1982**.
[66] J. T. Tsai, Y. S. Su, D. M. Wang, J. L. Kuo, J. Y. Lai, A. Deratani, *J. Membr. Sci.* **2010**, *362*, 360.
[67] A. V. Ryazanov, M. I. J. van Dijke, K. S. Sorbie, *Transp. Porous Media* **2009**, *80*, 79.
[68] J. Crank, *The Mathematics of Diffusion*, Oxford Science Publications, London **1976**.
[69] A. J. Boyle, A. C. Weems, S. M. Hasan, L. D. Nash, M. B. B. Monroe, D. J. Maitland, *Smart Mater. Struct.* **2016**, *25*, 075014.
[70] A. Matsumoto, N. Sato, T. Sakata, R. Yoshida, K. Kataoka, Y. Miyahara, *Adv. Mater.* **2009**, *21*, 4372.
[71] T. D. Nguyen, C. M. Yakacki, P. D. Brahmbhatt, M. L. Chambers, *Adv. Mater.* **2010**, *22*, 3411.
[72] W. Stober, A. Fink, E. Bohn, *J. Colloid Interface Sci.* **1968**, *26*, 62.

